Available online at www.sciencedirect.com
ScienceDirect
Trans. Nonferrous Met. Soc. China 32(2022) 3444−3458
Transactions of Nonferrous Metals Society of China
www.tnmsc.cn

Employing magnesium−lead melt for synergetic and selective extraction of copper from copper−cobalt alloy

Chun-xi ZHANG, Da-wei YU, Xue-yi GUO, Qing-hua TIAN

School of Metallurgy and Environment, Central South University, Changsha 410083, China

Received 15 August 2021; accepted 4 March 2022

Abstract: This research aims to extract Cu from Cu−Co alloy with high efficiency and selectivity by employing binary Mg−Pb melt. The optimal conditions for the extraction of Cu were determined. The results showed under optimal conditions, 96.5% of Cu in the Cu−Co alloy could be selectively extracted after treatment at 800 °C for 1 h, with the extraction rates of only 0.2% Fe, 0.6% Co, and 1.4% Si. The dissolution mechanism involved the counter diffusion of Mg/Pb and Cu across the diffusion zone of the Cu−Co alloy, and Mg in the binary Mg−Pb melt played a major role in the selective dissolution of Cu, especially at the dissolution forefront. The rate-controlling step of the extraction was dominated by the interfacial reaction.

Key words: Cu−Co alloy; Mg−Pb−Cu ternary system; selective dissolution; kinetics; dealloying

1 Introduction

Cobalt is a strategic metal with a variety of applications, such as rechargeable batteries [1], catalysts [2], pigment [3], magnets [4], super-alloys [5], and hard alloys [6]. Among them, the rechargeable batteries industry consumed 58% of the global cobalt in 2020 [7]. The future demand for cobalt will likely increase intensively to meet the great demand for electronic products and electric-powered vehicles [8,9]. Cobalt is a common element in nature, but its average content in the earth's crust is only about 17.3×10^{-6} (mass fraction) [10]. There is no individual cobalt mineral, and most cobalt is associated with Fe, Ni, and Cu [7]. The global cobalt resource reserves remain at about 7×10^{6} t, of which the Democratic Republic of Congo (DRC)'s cobalt resource reserve accounts for as much as 50% [11]. The cobalt mineralization in DRC is mainly in the form of Cu−Co oxide ores. Cu−Co alloy is produced by treating Cu−Co oxide ore with electric furnace reduction smelting. It is one of the primary Co-bearing materials for exportation instead of ore [12].

At present, the extraction of metals from Cu−Co alloy is principally by hydrometallurgical means. Because of its characteristics of corrosion resistance and high hardness, the dissolution step of Cu−Co alloy into aqueous solutions is challenging [13,14]. The dissolution methods of Cu−Co alloy can be divided into acid leaching, pressure leaching, and electrochemical dissolution. Usually, a certain amount of oxidant is required during the acid leaching process to increase the leaching rate of valuable metals, such as chlorine gas [15], H_2O_2 [16], and hydrofluoric acid [12]. Electrochemical dissolution was also studied, involving casting the Cu−Co alloy into an anode and using Cu plate as the cathode [17,18]. Direct acid leaching of Cu−Co alloy is difficult. Most leaching methods require pretreatment such as ball milling or spray granulation to reduce the particle size of Cu−Co alloy for better leaching efficiency.

Corresponding author: Da-wei YU, Tel: +86-731-88876255, E-mail: dawei.yu@csu.edu.cn
DOI: 10.1016/S1003-6326(22)66031-X

This pretreatment step dramatically increases the operating cost. The pyrometallurgical pretreatment was also studied to de-siliconize the Cu−Co alloy and destroy its refractory structure simultaneously, which is beneficial to the subsequent leaching process. JEONG et al [19] used calcium sulfate to roast the Fe−Ni−Cu−Co alloy and added carbon as a reducing agent. The alloy phase transformed into the Fe−Ni−Cu−Co−S matte phase. REN et al [20] used Mn_3O_4−MgO as a desiliconization medium and formed MnO−MgO−SiO_2 with the enhancement of oxidation by introducing O_2. This method can remove 84 wt.% of the silicon from the alloy.

Selective extraction of a metallic component from alloy-based materials using liquid metal is achieved by taking advantage of the solubility difference of various metal components in the liquid metal, which has become an effective method for alloy scrap recycling [21]. For example, the valuable Nd can be selectively extracted by molten Mg or Ag from Fe−Nd−B magnets [22], and Ni can be selectively extracted by molten Zn or Mg from nickel-based superalloys [23]. Aiming to address the above mentioned issues associated with the hydrometallurgical processing of Cu−Co alloy, we have recently reported an innovative method for the selective extraction of Cu from Cu−Co alloy by employing molten Mg as the extraction medium [24]. Subsequent vacuum distillation of the obtained molten Mg−Cu alloy realized the separation of Cu from molten Mg, which can be reused as the extraction medium. Although the extraction degree of 98.9% for Cu was achieved, molten Mg also exhibited specific solubility for Co, resulting in the co-extraction rate of approximately 5 wt.% Co. Cobalt ended in the obtained Cu powder after vacuum distillation, reducing its purity. In addition to Mg, Pb also has certain solubility for Cu according to the Pb−Cu phase diagram [25]. For example, molten Pb can dissolve approximately 10 at.% of Cu at 800 °C. Moreover, based on the binary Pb−Me phase diagrams (Me=Fe, Co, Si) [25], Fe, Co, and Si are essentially insoluble in molten Pb, indicating its excellent selectivity. Herein, we used the binary Mg−Pb melt as the extraction medium for synergetic and selective extraction of Cu from Cu−Co alloy, by combining the characteristics of the high selectivity of Pb and high capacity of Mg for Cu dissolution. Figure 1 shows the liquidus projection of the ternary Mg−Pb−Cu system, which was calculated using the thermochemical software

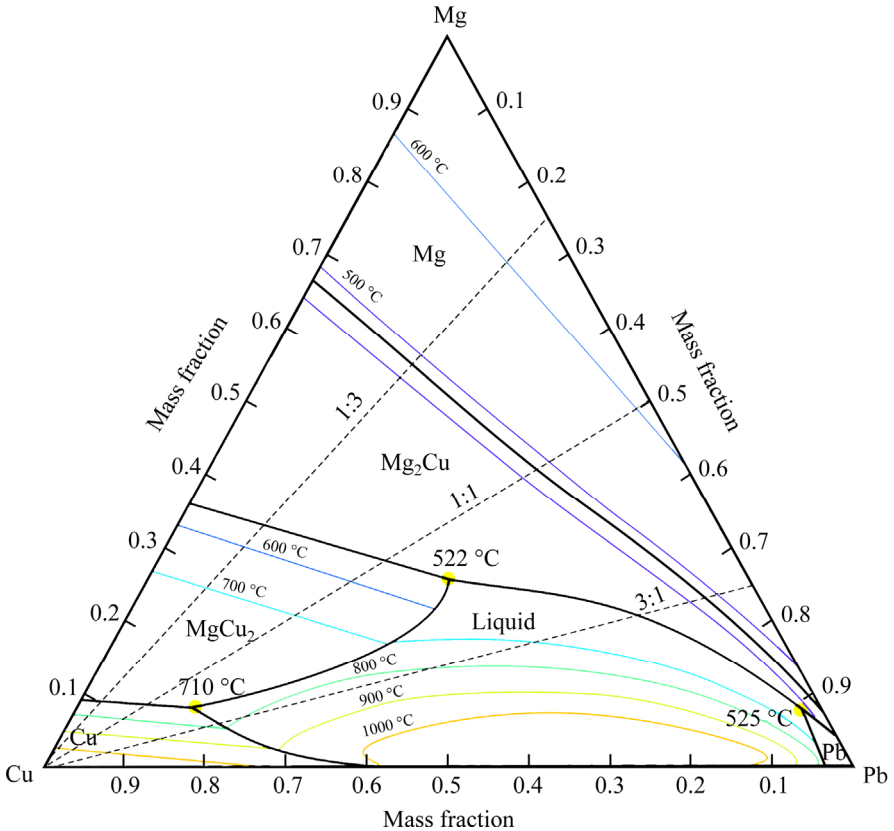

Fig. 1 Liquidus projection of ternary Mg−Pb−Cu system, calculated using FactSage 7.1 [26]

FactSage 7.1 [26], with its FScopp database. This figure demonstrates the extent of Cu dissolution by the Pb−Mg alloy under different mass ratios of Pb/Mg and temperatures. The three dotted lines in the figure represent the Pb/Mg mass ratios of 1:3, 1:1, and 3:1, respectively. With the continuous dissolution of Cu at a fixed Pb/Mg mass ratio, the liquid composition follows the dotted line toward the Cu corner with increasing Cu concentration. When treated at a constant temperature, the secondary phases (i.e., Mg_2Cu, $MgCu_2$, and Liquid) begin to form when the dotted line intersects with the corresponding isotherm. This demonstrates the high capacity for Cu dissolution by the binary Pb−Mg melt.

The proposed process for the selective extraction of Cu from Cu−Co alloy by molten Mg−Cu is illustrated in Fig. 2. The Cu−Co alloy is firstly treated with molten Pb−Mg for the selective extraction of Cu. After separating from the Fe−Co−Si residue, the obtained Mg−Pb−Cu alloy can be further subjected to vacuum distillation to obtain Cu and Mg−Pb alloy according to the relatively high vapor pressure of Mg and Pb [27], which is recycled for re-use. In this work, the selective extraction of Cu from Cu−Co alloy by the molten Pb−Mg was experimentally studied, focusing on the dissolution behavior of each element and the transformation of various phases. The kinetic study was also performed on the dissolution of Cu from Cu−Co alloy into the liquid Pb−Mg.

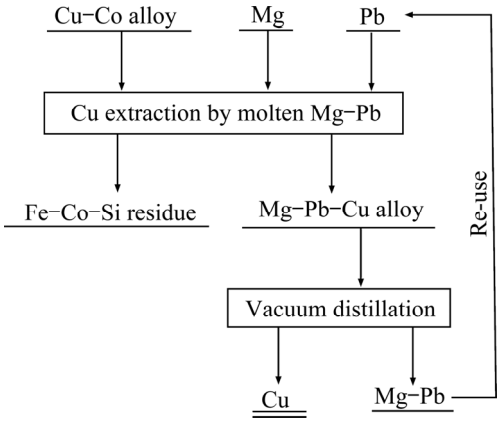

Fig. 2 Proposed process for extraction of Cu from Cu−Co alloy with molten Mg−Pb

2 Experimental

2.1 Preparation of Cu−Co alloy

The Cu−Co alloy with a uniform composition was prepared in the laboratory. High purity Cu, Co, Fe, and Si powders were firstly mixed thoroughly at a mass ratio of 3:3:3:1 before placing the mixed powders into a corundum crucible. The crucible and the metal powders inside were subsequently heated using an electric tube furnace at 1600 °C for 4 h with a continuous purging of 50 mL/min Ar gas (5N). The Cu−Co alloy ingot was obtained after cooling in the furnace. The alloy ingot was crushed into particles and sieved to produce a size range of 0.9−2 mm, which was used for the experimental study. Cuboids with dimensions of 5 mm × 5 mm × 10 mm were also prepared by cutting the Cu−Co alloy ingot, which were used for the kinetic study of the liquid metal extraction process. The chemical composition of the Cu−Co alloy was analyzed by inductively coupled plasma optical emission spectrometry (ICP-OES, Spectro Blue SOP, Germany). Morphological observations and composition analyses were performed using scanning electron microscopy (SEM, TESCAN MIRA3, Czech Republic) coupled with energy dispersive spectroscopy (EDS, Oxford XMAX20, UK). The accelerating voltage was 20 kV.

2.2 Cu extraction by molten Mg−Pb

The Cu−Co alloy particles, Mg shots, and Pb shots were mixed and put into a graphite crucible (inner diameter 22 mm; height 35 mm). The total mass of the sample was maintained at 12 g. The sample was then placed in a vertical tube furnace and heated at a heating rate of 15 °C/min to a predetermined temperature in the range of 750−900 °C, and kept at the temperature for 0−2 h. The experiment was carried out with the continuous purge of Ar gas (5N pure) with a flow rate of 50 mL/min. The sample was allowed to cool in the furnace to form an alloy ingot. The obtained alloy ingot was residual Fe−Co−Si particles surrounded by solidified Mg−Pb−Cu alloy. The alloy ingot was cut into halves along the longitudinal direction, and the cross-section of one-half was polished by emery papers. The morphological observations and composition analyses were performed using SEM coupled with EDS.

The Mg−Pb−Cu alloy was obtained by cutting off the part of the sample ingot which did not contain Fe−Co−Si residue. And the Fe−Co−Si residue was obtained by leaching the sample ingot with 1 mol/L acetic acid to selectively dissolve the

Mg−Pb−Cu phase. The chemical compositions of the Mg−Pb− Cu alloy and Fe−Co−Si residue were analyzed by ICP-OES. By analyzing the chemical compositions of the Mg−Pb−Cu alloy and Fe−Co−Si residue, the extraction rate of each element can be calculated.

A method similar to the one used in our earlier investigation [21] was adopted to calculate the extraction rate of each element. The extraction rate of each element M can be calculated using Eq. (1):

$$\eta_{\mathrm{M}} = \frac{m_{\mathrm{Mg-Pb-Cu}} \cdot w^{\mathrm{M}}_{\mathrm{Mg-Pb-Cu}}}{m_{\mathrm{Mg-Pb-Cu}} \cdot w^{\mathrm{M}}_{\mathrm{Mg-Pb-Cu}} + m_{\mathrm{residue}} \cdot w^{\mathrm{M}}_{\mathrm{residue}}} \times 100\% \quad (1)$$

where η_{M} represents the extraction rate of each element M (M=Fe, Co, Si), $m_{\mathrm{Mg-Pb-Cu}}$ is the mass of Mg−Pb−Cu alloy, $w^{\mathrm{M}}_{\mathrm{Mg-Cu-Pb}}$ is the mass fraction of element M in the Mg−Pb−Cu alloy, m_{residue} is the mass of the alloy residue, and $w^{\mathrm{M}}_{\mathrm{residue}}$ is the mass fraction of element M in the alloy residue.

2.3 Dissolution mechanism and kinetic study

The diffusion couple method was used to investigate the dissolution mechanism and kinetics of the liquid metal extraction process. The Cu−Co alloy cuboids (dimensions: 5 mm × 5 mm × 10 mm; mass: 1.8 g) and cubic Mg−Pb ingot (dimensions: 10 mm × 10 mm × 10 mm; mass: 4.5 g) were used. The mass ratio of Pb to Mg in the Mg−Pb ingot was 3:1, and the mass ratio of Cu−Co alloy to Mg−Pb ingot was 2:5. To ensure that only one surface of the Cu−Co alloy cuboid gets in contact with the molten Mg−Pb, the Cu−Co alloy was tightly fitted into a U-shaped graphite block. Then, the graphite block, the Cu−Co alloy and the Mg−Pb ingot were put into a graphite crucible before placing them in the cold zone of the electric furnace. After the furnace reached the target temperature, the crucible and the sample were pushed using a pushing rod into the heating zone of the furnace to allow for instant heating. After heating for a predetermined time, the sample was pulled back to the cold zone using the pushing rod. The push-and-pull mechanism ensured the precise control of the extraction time, which is critical in the kinetic study. A continuous flow of 50 mL/min Ar gas (5 N) was maintained throughout the experiment. The obtained sample was vertically cut, and the cross-section of the sample was polished by emery papers. Morphological observations and composition analyses were performed using SEM coupled with EDS.

3 Results and discussion

3.1 Characterization of Cu−Co alloy

The chemical composition of the Cu−Co alloy prepared in the laboratory is shown in Table 1. Figure 3(a) shows the BSE image of the Cu−Co alloy. It can be seen that the alloy contains two major phases. Figures 3(b) and (c) show the EDS spectra of Areas 1 and 2 in Fig. 3(a), respectively. According to the EDS results, the lighter gray phase is the Cu-rich phase, and the dark matrix is rich in Fe, Co, and Si.

Table 1 Chemical composition of prepared Cu−Co alloy (wt.%) [21]

Co	Fe	Cu	Si
33.8	33.3	21.8	11.1

3.2 Extraction of Cu from Cu−Co alloy using molten Mg−Pb

3.2.1 Effect of mass ratio of Pb to Mg

The influence of the mass ratio of Pb to Mg (m_{Pb}:m_{Mg}) variation (1:0, 3:1, 1:1, 1:3, 0:1) was firstly investigated. Other experimental parameters maintained the same for a series of experiments, which were as follows: Cu−Co alloy particle size 0.9−2 mm, m_{alloy}:$m_{\mathrm{Mg-Pb}}$=1:5, processing temperature 850 °C, and processing time 1 h. Figure 4 shows the effect of the mass ratio of Pb to Mg on the extraction rates of Cu, Co, Fe, and Si. As seen, when pure Pb was used as the extractant (i.e., m_{Pb}:m_{Mg}=1:0), the extraction rate of Cu was only 4%, demonstrating its limited capacity for Cu dissolution. At the m_{Pb}:m_{Mg} of 3:1, the extraction rate of Cu increased rapidly to 94.4%. With the further increase of the Mg content in the molten Pb−Mg, the extraction rate of Cu increased slowly. The extraction rate of Co was also influenced by m_{Pb}:m_{Mg}. A substantial increase in the Co extraction rate can be seen when m_{Pb}:m_{Mg} reached 1:1, suggesting its lower selectivity for Cu extraction. Surprisingly, the extraction rate of Si was as high as 20.9% when using pure Pb (i.e., m_{Pb}:m_{Mg}=1:0) since the solubility of Si in liquid Pb is negligible at the temperature of investigation, based on the Pb−Si binary phase diagram [28].

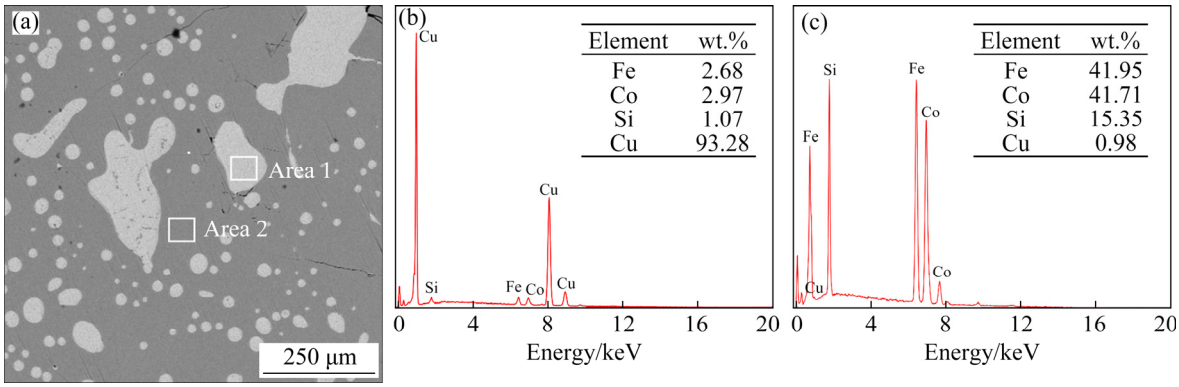

Fig. 3 BSE image of Cu−Co alloy (a) and EDS spectra and compositions of Area 1 (b) and Area 2 (c) in (a)

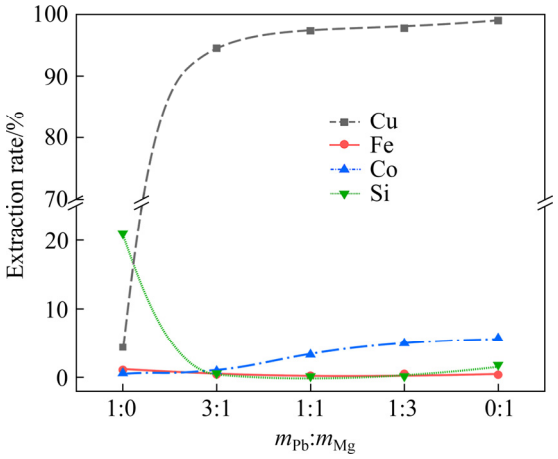

Fig. 4 Effect of m_{Pb}:m_{Mg} on extraction rates of Cu, Fe, Co, and Si into molten Pb−Mg

Figure 5 shows the BSE images and elemental mapping micrographs of the boundary between Cu−Co alloy residue and the solidified Pb−Mg alloy with varying m_{Pb}:m_{Mg} ratio. The region on the left of each micrograph is the solidified melt, and the region on the right is the residual Cu−Co alloy. At the m_{Pb}:m_{Mg} of 1:0, a reaction layer formed between the alloy and melt. As evidenced by the elemental mapping of the micrograph, the reaction layer comprised two sub-layers: one contained Co, Fe, and Pb, the other was rich in Si. The Si content in the second sub-layer layer was higher than that in the residual alloy, suggesting an outward migration of Si from the interior of the Cu−Co alloy. Micro-grains of the Si-bearing phase were highly dispersed in the Pb melt, which coincides with the high Si extraction rate, as shown in Fig. 4. It is surprising because Si is essentially insoluble in liquid Pb at the temperature of investigation based on the Pb−Si binary phase diagram [28]. This is tentatively suggested as the result of the presence of residual oxygen (Refer to the Pb−O phase diagram [29]) in the starting Pb. At 850 °C, the dissolved O in liquid Pb likely reacted preferentially with Si that migrated out from the Cu−Co alloy, because the affinity of Si to O is stronger than that of Pb, Fe, Co, and Cu to O. The reaction can be represented by Reaction (2). The formed SiO_2 dispersed in the Pb melt, as seen in the elemental mapping of Si in Fig. 5(a). The oxidization of Si and the dissolution of Cu in liquid Pb resulted in the splintering of the Cu−Co alloy and formed the reaction layer. Comparatively, Si was not observed in the melt region with the presence of Mg in the melt (Figs. 5(b−e)). Because the affinity of Mg to O is stronger than that of Si to O, the dissolved O in the molten Pb preferentially reacted with Mg to form MgO when the extractant contained Mg, thereby preventing the oxidation of Si.

$$[O]_{Pb}+Si=SiO_2 \quad (2)$$

In the presence of Mg in the melt, no reaction layer was formed, and the Cu−Co alloys were entirely penetrated by the extractant, as shown in Figs. 5(b−e). Based on the elemental mapping of Cu, most Cu resided in the melt region in the presence of Mg, conforming with the high Cu extraction rates as shown in Fig. 4.

Based on the above analysis, when pure Pb was used as the extractant, the selective dissolution of Cu was slow, and a certain amount of Si could be oxidized by the dissolved O in liquid Pb, forming SiO_2 particles which dispersed in the molten Pb. When pure Mg was used as the extractant, the dissolution was efficient, and a high extraction rate of Cu could be obtained, but a small amount of Co was also extracted by molten Mg. Excellent

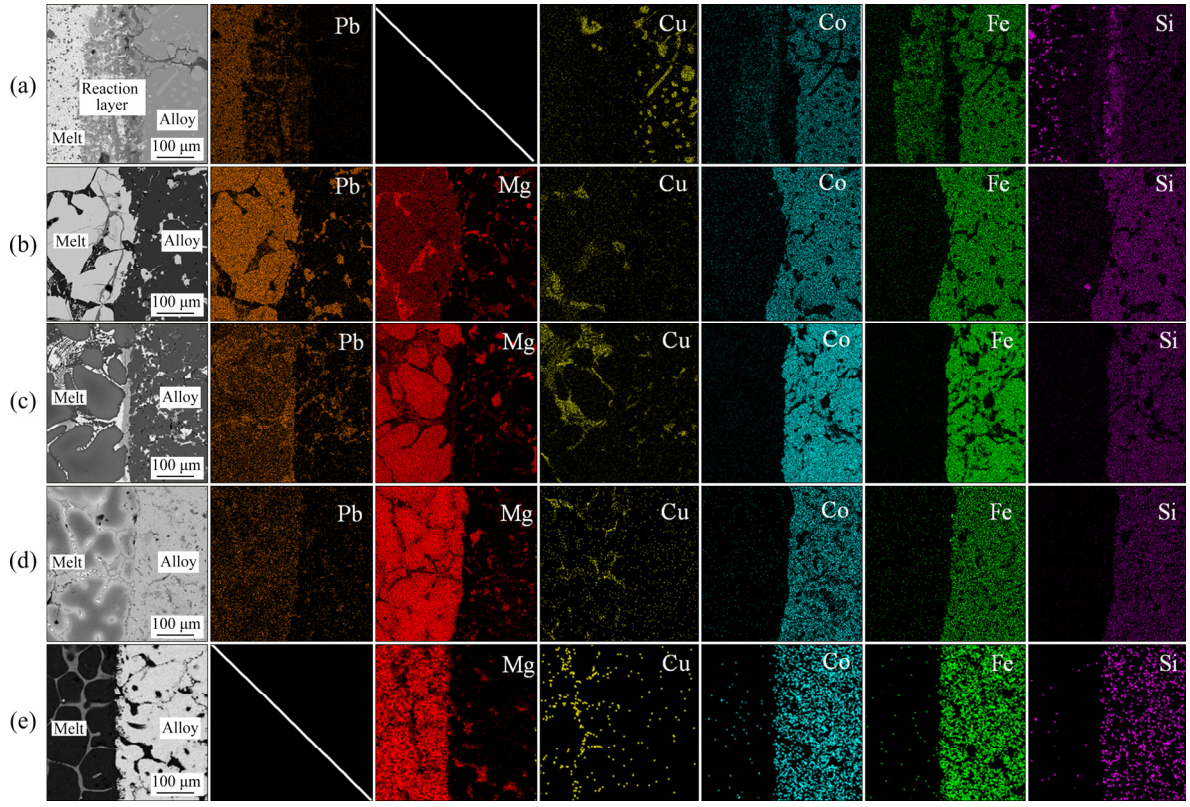

Fig. 5 BSE images and elemental mapping micrographs of boundaries between Cu−Co alloy residue and solidified Pb−Mg alloy after liquid metal extraction using molten Mg−Pb with varying m_{Pb}:m_{Mg} ratios: (a) 1:0; (b) 3:1; (c) 1:1; (d) 1:3; (e) 0:1

selectivity could be achieved using a m_{Pb}:m_{Mg} of 3:1. The presence of Mg realized the effective dissolution of Cu and prevented the oxidation of Si, and the presence of Pb minimized the dissolution of Co. Therefore, m_{Pb}:m_{Mg}=3:1 was chosen as the best mass ratio of Pb to Mg.

3.2.2 Effect of temperature

The influence of temperature was studied in the range of 750−950 °C. Other experimental parameters remained the same as follows: Cu−Co alloy particle size 0.9−2 mm, m_{alloy}:m_{Mg-Pb}=1:5, m_{Pb}:m_{Mg}=3:1 and processing time 1 h. Figure 6 shows the effect of the processing temperature on the extraction rates of Cu, Fe, Co, and Si. As seen, the processing temperature exhibits a limited effect on the extraction rates of Fe, Co, and Si. When the processing temperature changed from 750 to 800 °C, the extraction rate of Cu rose from 84.3% to 96.5%. The extraction rate of Cu, as well as Fe, Co, and Si remained unchanged with the further increase of temperature.

Figure 7 shows the BSE images and elemental mapping micrographs of the Cu−Co alloy residue

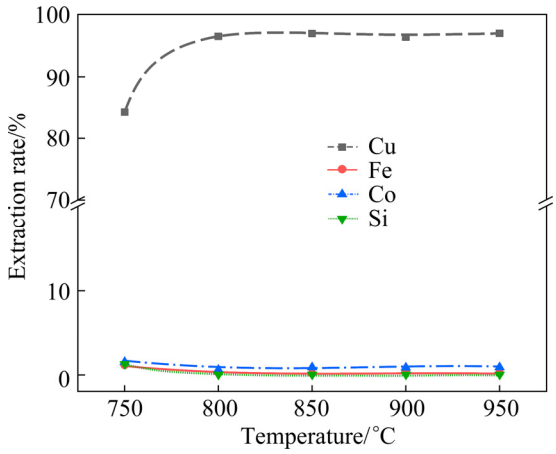

Fig. 6 Influence of temperature on extraction rates of Cu, Fe, Co, and Si

obtained from the Cu−Co alloys treated with molten Mg−Pb at 750, 800, 850, and 900 °C. It can be seen from Fig. 7(a) that after treating at 750 °C, the alloy residue still contained a Cu-rich phase (outlined by a blue dotted ellipse), which was disseminated in the Fe−Co−Si matrix. This indicated the dissolution of Cu from the Cu−Co alloy by the molten Mg−Pb was still far from completion, which conforms with

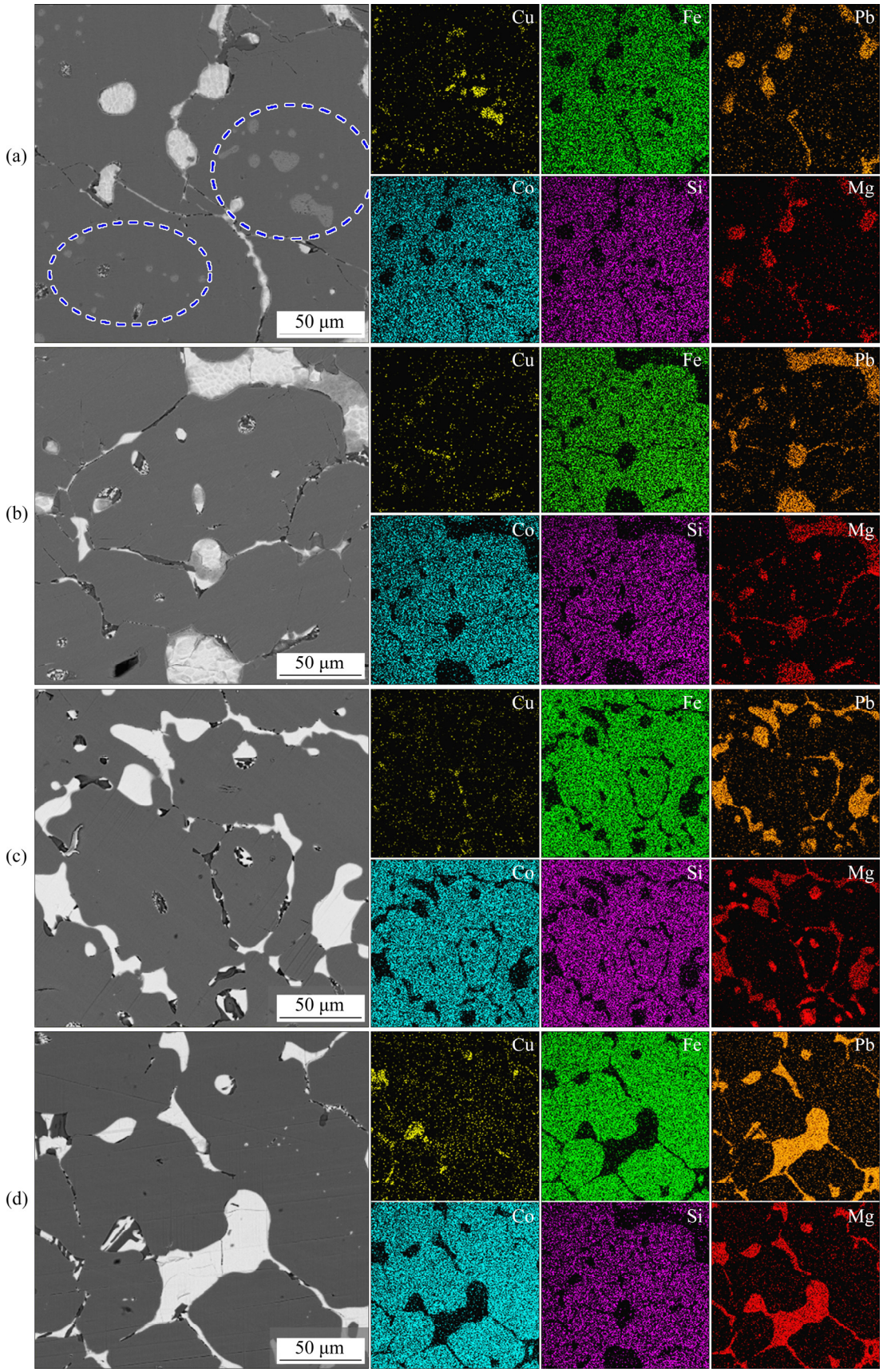

Fig. 7 BSE images and elemental mapping micrographs of Cu−Co alloy residue after liquid metal extraction using molten Mg−Pb at 750 °C (a), 800 °C (b), 850 °C (c), and 900 °C (d)

the relatively low Cu extraction rate, as shown in Fig. 6. The influencing mechanism of temperature on the extraction can be a combination of two main aspects, i.e., the solubility of Cu in molten Mg−Pb (thermodynamics), and the Cu diffusion rate in Cu−Co alloy as well as in the molten Mg−Pb (kinetics). According to the liquidus projection of the Mg−Pb−Cu system as shown in Fig. 1, at 750 °C and with a m_{Pb}:m_{Mg} ratio of 3:1, continuous dissolution of Cu results in the formation of a secondary liquid phase (denoted as Liquid) after reaching approximately 30 wt.% Cu in Mg−Pb−Cu, suggesting a high solubility of Cu. Theoretically, 2.5 g Mg and 7.5 g Pb, which were used in this experiment, could dissolve all Cu present in the 2 g Cu−Co alloy. Therefore, it can be inferred that the limited Cu diffusion rate was the main reason for restricted extraction, rather than the solubility of Cu in the Mg−Pb melt.

Low processing temperature of 750 °C would likely result in a slower diffusion rate of Cu from Cu−Co alloy into the molten Mg−Pb, leading to the presence of Cu-rich phase in the Cu−Co alloy residue and the incomplete extraction of Cu within 60 min. It can be seen from Figs. 7(b−d) that the Cu-rich phase was not observed when the processing temperature was no less than 800 °C, indicating that the extraction was close to completion. Figure 6 suggests the extraction rate of Cu plateaued at around 96%. As seen from the BSE images of the alloy residue and the corresponding elemental mapping micrographs (Figs. 7(b−d)), the Cu present in the Cu−Co alloy residue was mainly in the form of an Mg−Pb−Cu alloy phase. The likely-molten Mg−Pb−Cu alloy phase exhibited an inter-connected network structure within the Cu−Co alloy residue, accounting for an accelerated mass transport within the solid alloy residue. After the diffusion and dissolution reached equilibrium, the concentration of Cu in the Mg−Pb melt, which penetrated into the alloy residue, would be consistent with the concentration of Cu in the Mg−Pb melt outside the alloy residue. The Mg−Pb−Cu phase remained in the alloy residue upon solidification, accounting for the 4 wt.% Cu that was not extracted (Fig. 6). Therefore, 800 °C was chosen as the optimal temperature for the selective extraction of Cu from Cu−Co alloy by Mg−Pb melt.

3.2.3 Effect of mass ratio of Cu−Co alloy to Mg−Pb melt

The influence of the varying mass ratio of Cu−Co alloy to Mg−Pb melt m_{alloy}:m_{Mg-Pb} ratio (1:2, 1:5, 1:7, 1:9) on the selective extraction of Cu from Cu−Co alloy was studied by fixing other experimental parameters as follows: Cu−Co alloy particle size 0.9−2 mm, m_{Pb}:m_{Mg}=3:1, temperature 800 °C, and time 1 h. Figure 8 shows the effect of m_{alloy}:m_{Mg-Pb} on the extraction rates of Cu, Fe, Co, and Si. It can be seen that there is an apparent increase in the Cu extraction rate in the presence of more Mg−Pb. The extraction rates of Co and Si also exhibit a slightly increasing trend, while the extraction rate of Fe remains at about 0%.

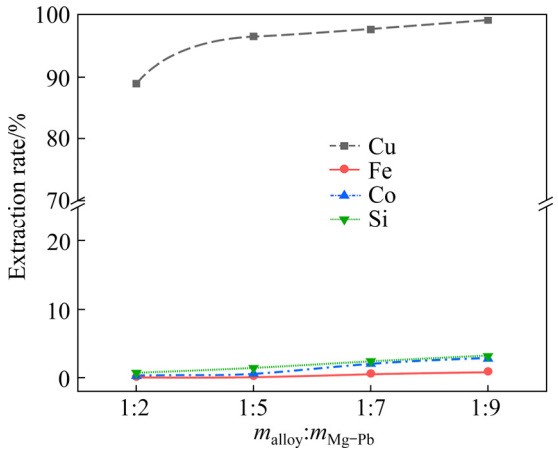

Fig. 8 Influence of m_{alloy}:m_{Mg-Pb} on extraction rates of Cu, Fe, Co, and Si

Figure 9 shows the BSE images and elemental mapping micrographs of the obtained products at different m_{alloy}:m_{Mg-Pb} ratios. As seen from Fig. 9(a), the Cu-rich phase can be observed in the residual alloy (highlighted with a red circle), which contained about 92 wt.% Cu based on EDS analysis. Due to the presence of smaller amounts of Mg−Pb (i.e., larger m_{alloy}:m_{Mg-Pb} ratio), the obtained Mg−Pb−Cu melt would contain higher concentration of Cu. Upon solidification, the Mg−Pb−Cu melt formed a Pb-rich phase (bright region) and a eutectic (light grey region) containing about 19 wt.% Cu, which took place in the melt pool as well as inside the residual alloy. The presence of Cu-rich phase (highlighted with a red circle in Fig. 9(a)) and Cu-bearing eutectic (highlighted with a blue circle) in the alloy residue resulted in a relatively low Cu extraction rate (i.e., 88.9 wt.%) at m_{alloy}:m_{Mg-Pb} ratio of 1:2.

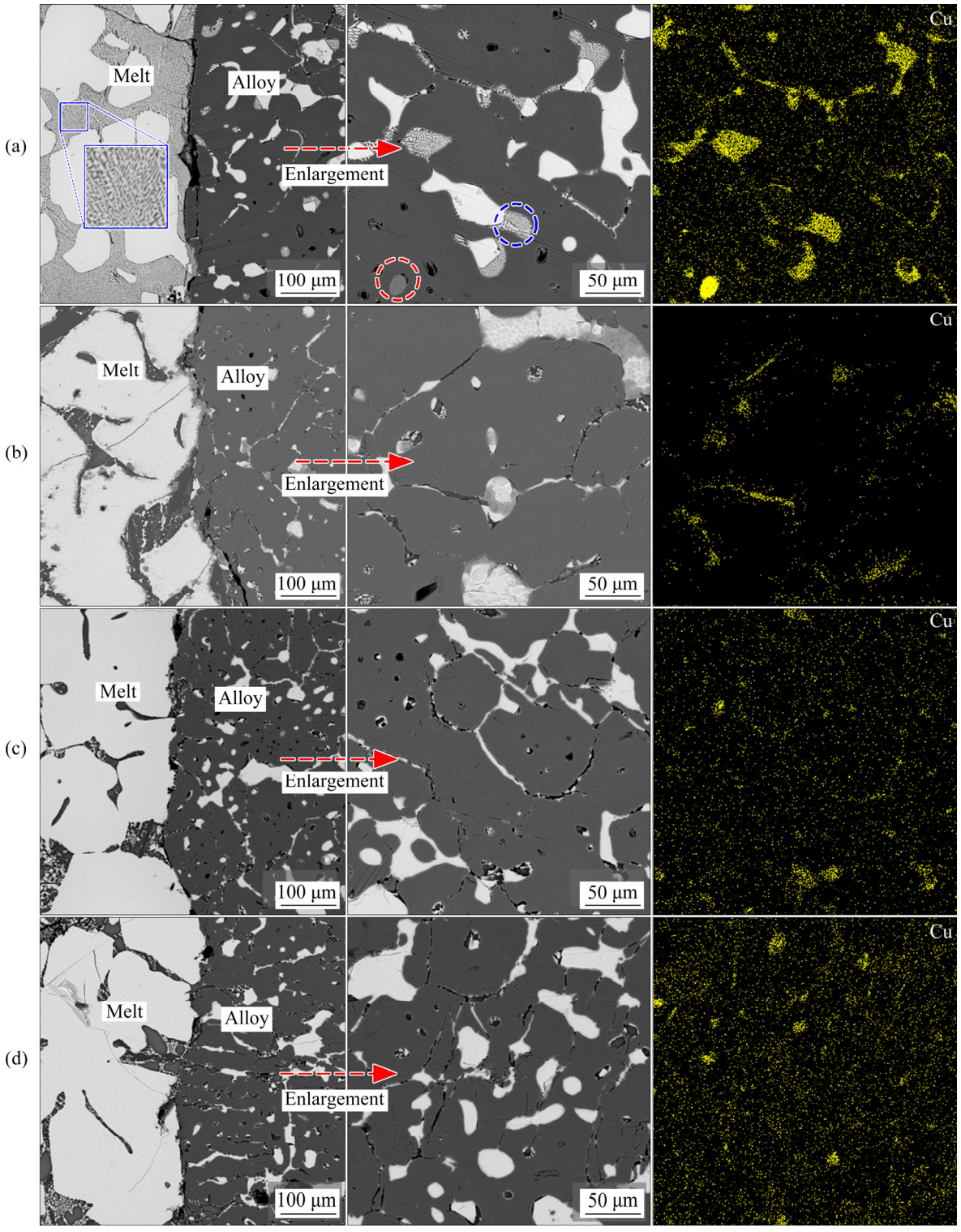

Fig. 9 BSE images of boundary between Cu−Co alloy residue and solidified Mg−Pb−Cu melt, enlarged BSE micrographs of alloy residue, and corresponding elemental mappings of Cu at different m_{alloy}:m_{Mg-Pb} ratios: (a) 1:2; (b) 1:5; (c) 1:7; (d) 1:9

With the increasing addition of Mg−Pb to m_{alloy}:m_{Mg-Pb} of 1:5, more extractant was provided for the dissolution of Cu from the Cu−Co alloy. As seen from Fig. 9(b), the Cu concentration in the Mg−Pb melt was effectively reduced, and there was no Cu-rich phase in the alloy residue. But the presence of solidified Mg−Pb−Cu melt in the alloy residue still contained a small amount of Cu.

With a further increase of Mg−Pb addition (i.e., m_{alloy}:m_{Mg-Pb}=1:7 and 1:9), the amount of Cu in the residual alloy was reduced, resulting in a rise in Cu extraction rate to 97.6% and 99%, respectively. However, a higher amount of Mg−Pb melt also facilitated the dissolution of Co and the oxidation of Si. At m_{alloy}:m_{Mg-Pb} of 1:7, the extraction rates of Co and Si were 1.9% and 2.4%, respectively. They further increased to 2.7% and 3.1%, respectively, at m_{alloy}:m_{Mg-Pb} of 1:9. Therefore, a high amount of Mg−Pb reduced the selectivity. In comparison, the extraction rates of Co and Si were only 0.5% and 1.4%, respectively, and the Cu extraction rate reached 96.5% at m_{alloy}:m_{Mg-Pb} of 1:5. Therefore, m_{alloy}:m_{Mg-Pb} of 1:5 was chosen as the optimized ratio and was used for the subsequent experiments.

3.2.4 Effect of extraction time

The effect of extraction time was evaluated after applying the experimental parameters that have been optimized, i.e., Cu−Co alloy particle size 0.9−2 mm, m_{Pb}:m_{Mg}=3:1, m_{alloy}:m_{Mg-Pb}=1:5, and processing temperature 800 °C. Figure 10 shows the effect of the extraction time on the extraction rates of Cu, Fe, Co, and Si. It can be seen that the extraction time had little influence on the extraction rates of Fe, Co, and Si, which remained close to zero. With increasing extraction time, the extraction rate of Cu exhibited a sharp increase in the early stage and reached a plateau of about 96% when the extraction time exceeded 60 min. Therefore, the optimum treatment time for the selective extraction of Cu from Cu−Co alloy by molten Mg−Pb was 60 min.

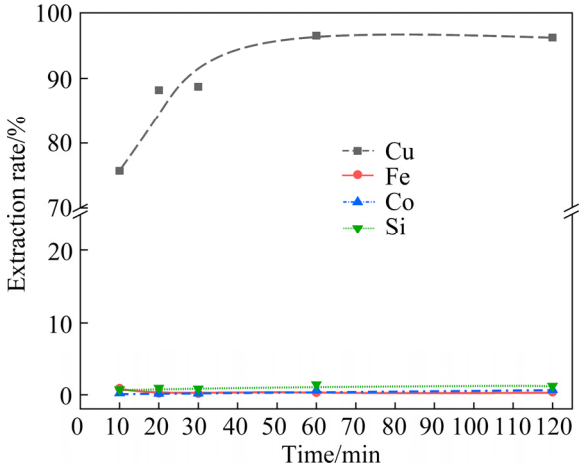

Fig. 10 Influence of time on extraction rates of Cu, Fe, Co, and Si

3.3 Dissolution mechanism and kinetic analysis

The diffusion couple of "Cu−Co alloy/Mg−Pb alloy" was used to investigate the dissolution mechanism and kinetics. After extraction, the obtained Cu−Co alloy cuboids were cut longitudinally, and the BSE images of the cross-sections are shown in Fig. 11. The left edge of each BSE image is the contact surface between the Cu−Co alloy and Mg−Pb melt. It can be observed that a diffusion zone was formed with varying thicknesses, initiating from the contact surface. This diffusion zone was characterized by the presence of the Pb−Mg phase (bright appearance). The right of the diffusion zone was the unreacted zone that was not yet corroded by the Mg−Pb melt. As seen, the thickness of the diffusion zone increased with the increase of extraction time and extraction temperature.

Closer observation on the phase and elemental distribution across the diffusion couple interface could help reveal the dissolution mechanism. Figure 12 shows the BSE images of the interface between the Cu−Co alloy and the Mg−Pb melt after reaction for 60, 90, and 120 min at 900 °C, which were superimposed with the concentration profiles of each element. The concentrations of Fe, Co, and Si in the unreacted and diffusion zones remained relatively unchanged, and their concentrations in the Mg−Pb zone were essentially zero. This demonstrated the high selectivity of Mg−Pb melt that minimized the dissolution of Fe, Co, and Si. A sharp decrease in the concentrations of Mg and Pb could be observed across the interface. Their concentrations gradually decreased inside the diffusion zone when moving away from the interface and finally reached zero after approaching the unreacted zone. An opposite concentration gradient can be observed for Cu across the diffusion zone. The concentration gradients across the diffusion zone within the Cu−Co alloy strongly suggest the mechanism involving the counter diffusion of Mg/Pb and Cu, allowing the Cu dissolution into the Mg−Pb pool outside the Cu−Co alloy. The volume reduction of the Cu−Co alloy resulting from the Cu dissolution created voids/channels for the inward penetration of the Mg−Pb melt, which resulted in the formation of interconnected networks of the Mg−Pb−(Cu) melt in the diffusion zone (as seen in Figs. 7, 9 and 12). The formation of the melt network in the diffusion

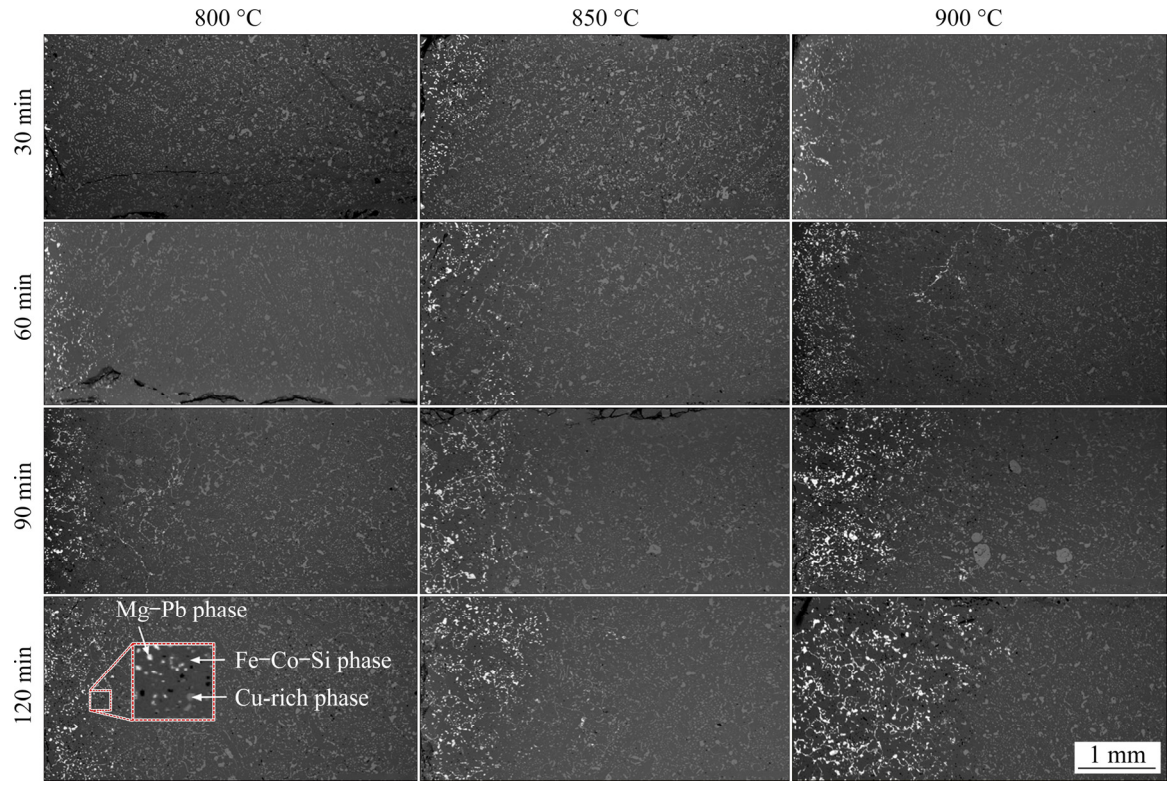

Fig. 11 BSE images of cross-sections of obtained Cu−Co alloy cuboids after extraction at different temperatures for different time (The left edge of each image is the contact surface between the Cu−Co alloy and the Mg−Pb melt. The bright dotted phase is the Mg−Pb phase, the lighter gray phase is the Cu-rich phase, and the dark gray matrix phase is the Fe−Co−Si phase)

zone allowed the enhanced counter diffusion of Mg/Pb and Cu, accounting for the fast dissolution kinetics. It can also be observed that the Cu concentrations on both sides of the interface generally became equal after treatment for 60 min. Further increase in treatment time to 90 and 120 min resulted in a higher local Cu concentration on the Mg−Pb side adjacent to the interface than that on the Cu−Co alloy side. This demonstrates the strong thermodynamic driving force for the Cu dissolution by Mg−Pb melt from the Cu−Co alloy.

The continuous counter diffusion of Mg/Pb and Cu across the diffusion zone accompanied the phase evolution. Figures 13(a−d) show the higher magnification BSE images of Regions (*A*−*D*) in Fig. 12(b), respectively. And the EDS results are shown in Table 2. As shown in Fig. 13, the phase transformation mainly involved Mg/Pb/Cu-bearing phases. According to the phase diagram of Mg−Cu [30], intermetallic compounds $MgCu_2$ and Mg_2Cu could be possibly formed during cooling and solidification. The molar ratio of Mg to Cu is close to 1:2 at Point 1 (see Table 2). Therefore, the phase of Point 1 in Fig. 13(a) is identified as $MgCu_2$. The regions represented by Points 2, 3, and 4 are characteristic of a eutectic structure composed of two alternating phases. According to the molar ratios of Mg, Pb, and Cu as shown in Table 2 and the phase equilibria of the Mg−Cu−Pb system [31], it can be deduced that the eutectic is binary Mg_2Cu−Mg_2Pb. The molar ratio of Mg to Pb of the bright phase represented by Points 5 and 6 is close to 2:1, indicating that this phase is Mg_2Pb. The dominant presence of $MgCu_2$ in Fig. 13(a), Mg_2Cu−Mg_2Pb eutectic in Figs. 13(b, c), and Mg_2Pb in Fig. 13(d), and taking into consideration of their relative locations in the diffusion zone (Fig. 12(b)), the following phase evolution within the diffusion zone became obvious when moving away from the diffusion couple interface: Mg_2Pb → Mg_2Cu−Mg_2Pb eutectic → $MgCu_2$. This suggested that Mg in the binary Mg−Pb melt played a major role in the selective dissolution of Cu, especially at the forefront of dissolution (i.e., close to the boundary between the diffusion zone and the unreacted zone, Region *A* in Fig. 12(b) for example).

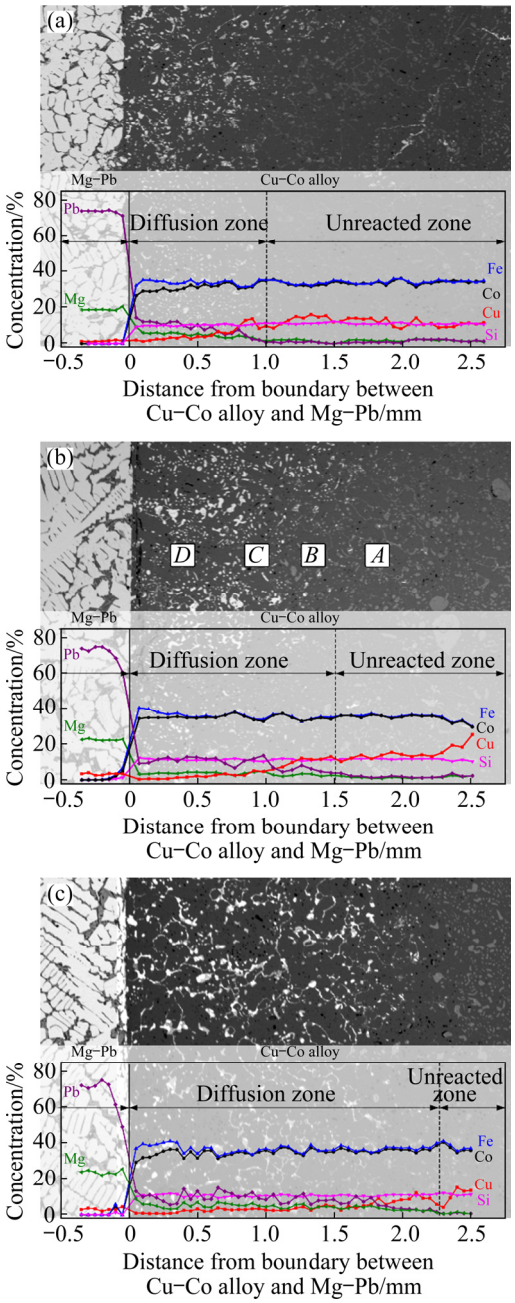

Fig. 12 BSE images showing boundary between Cu−Co alloy and Mg−Pb melt after reaction for 60 min (a), 90 min (b), and 120 min (c) at 900 °C, and corresponding concentration profiles of elements across boundary

Kinetic analysis was performed using the same approach employed in our earlier study [21] by quantifying the average thickness of the diffusion zone. The average thickness l_x of the diffusion zone of sample x shown in Fig. 11 was calculated based on Eq. (3):

$$l_x = A_x / W_x \tag{3}$$

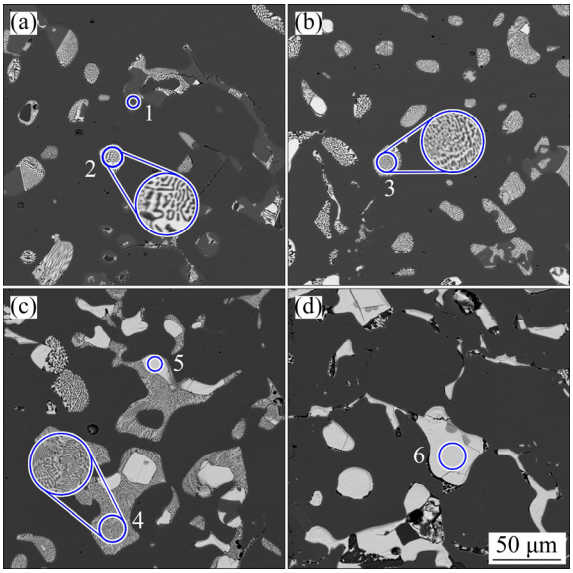

Fig. 13 Cross-sectional BSE images of Regions *A* (a), *B* (b), *C* (c), and *D* (d) in Fig. 12(b)

Table 2 EDS chemical compositions of points marked in Fig. 13

Point No.	Content/at.%						Phase
	Cu	Co	Fe	Si	Pb	Mg	
1	62.96	2.15	1.41	1.98	0.05	31.45	$MgCu_2$
2	20.58	1.28	1.12	0.34	13.51	63.18	Mg_2Cu–Mg_2Pb eutectic
3	20.78	1.77	1.37	0.18	13.75	62.14	Mg_2Cu–Mg_2Pb eutectic
4	21.20	0.65	0.49	0.29	14.88	62.49	Mg_2Cu–Mg_2Pb eutectic
5	0.57	0.79	1.70	1.79	33.81	61.34	Mg_2Pb
6	0.29	0.96	0.77	0.48	34.03	63.47	Mg_2Pb

where W_x represents the width of the Cu−Co alloy, which is 5 mm, and A_x is the area of the diffusion zone on the cross-section of the sample, measured using the image processing software ImageJ [32]. The calculated results are shown in Table 3 and Fig. 14. As seen, the thickness of the diffusion zone increased with increasing both the reaction time and temperature. The thickness l_x is a function of time t, expressed as Eq. (4) [33]:

$$l_x = k\left(t/t_0\right)^n \tag{4}$$

where t represents the reaction time, t_0 represents

the unit time, 1 s, to obtain a normalized dimensionless time, k represents the rate constant, and n represents the reaction exponent. The value of reaction exponent n indicates the type of the rate-controlling step. When n=0.5, the rate is diffusion-controlled, while n value of 1 represents that the rate is interfacial reaction-controlled [34,35]. The obtained n values are 1.238, 0.952, and 0.892, for temperatures of 800, 850, and 900 °C, respectively. This indicates that the rate-controlling step of the extraction reaction was dominated by interfacial reaction at the three temperatures of investigation. By referring to the dissolution mechanism which was discussed above, Cu dissolution into the Mg-rich melt, taking place at the forefront of dissolution (i.e., close to the boundary between the diffusion zone and the unreacted zone, Region *A* in Fig. 12(b) for example), was likely the rate-controlling step.

Table 3 Thicknesses of samples calculated using Eq. (3)

T/°C	t/min	l_x/μm
800	30	182.2
	60	344.2
	90	720.2
	120	968.2
850	30	399.8
	60	938.6
	90	1193
	120	1381.8
900	30	643.2
	60	1057.6
	90	1564.4
	120	2275.4

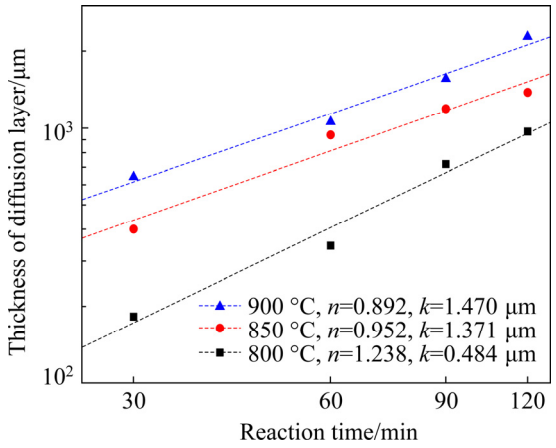

Fig. 14 Thickness of diffusion zone versus reaction time at 800, 850 and 900 °C

The associated apparent activation energy E_a can be calculated by applying the Arrhenius equation (Eq. (5)) [33], which expresses the relationship between the rate constant k and the activation energy E_a:

$$k = k_0 \exp[-E_a/(RT)] \quad (5)$$

where k_0 is the pre-exponential factor, and R is the molar gas constant. Figure 15 shows plots of ln k versus the reciprocal temperature. The activation energy can be calculated from the slope of the linear fitting, and an E_a value of 117.7 kJ/mol was obtained.

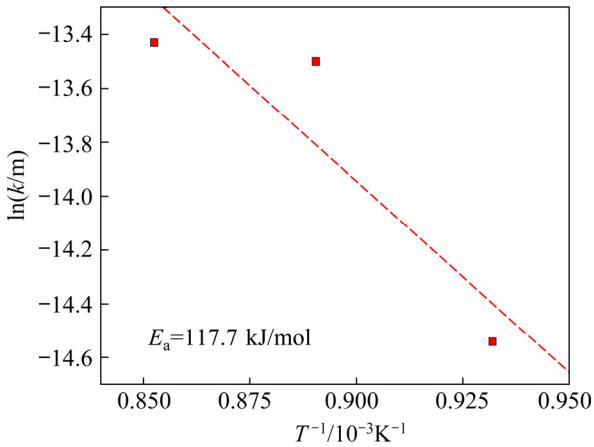

Fig. 15 Plot of ln k versus $1/T$

4 Conclusions

(1) The role of Mg and Pb in the Mg−Pb binary melt was synergetic toward the selective extraction of Cu from the Cu−Co alloy. The presence of Mg in the melt ensured a high Cu extraction rate because of its high capacity for Cu dissolution in the temperature range of investigation. The presence of residual O in the starting Pb resulted in a relatively high Si extraction rate (i.e., 20.9% at 850 °C) through oxidation, if the unary Pb melt was used. The use of binary Mg−Pb melt prevented the possible oxidation of Si, thereby minimizing the extraction of Si. Pb in the binary melt helped suppress the dissolution of Co, thus improving the selectivity.

(2) The optimal experimental conditions are m_{Pb}:m_{Mg}=3:1, extraction temperature of 800 °C, m_{alloy}:m_{Mg-Pb}=1:5, and extraction time of 1 h. Under these conditions, the extraction rate of Cu reached

96.5%. And the extraction rates of Fe, Co, and Si were only 0.2%, 0.6%, and 1.4%, respectively. This shows the high effectiveness and selectivity for Cu extraction from the Cu−Co alloy by employing molten Mg−Pb.

(3) Volume reduction of the Cu−Co alloy resulting from the Cu dissolution created voids/channels that allowed the inward penetration of the Mg−Pb melt, which resulted in the formation of interconnected networks of the Mg−Pb−(Cu) melt in the diffusion zone. The counter diffusion of Mg/Pb and Cu across the diffusion zone of the Cu−Co alloy resulted in the Cu dissolution into the Mg−Pb pool outside the Cu−Co alloy. The following phase evolution within the diffusion zone can be observed: Mg_2Pb → Mg_2Cu−Mg_2Pb eutectic → $MgCu_2$, suggesting that Mg in the binary Mg−Pb melt played a major role in the selective dissolution of Cu, especially at the forefront of dissolution.

(4) In the temperature range of 800−950 °C, the rate-controlling step of the extraction was dominated by the interfacial reaction. The apparent activation energy of the selective Cu dissolution from Cu−Co alloy by molten Mg−Pb was estimated to be 117.7 kJ/mol.

Acknowledgments

This research was funded by the National Natural Science Foundation of China (Nos. 51904350, 51874371), and the Hunan Natural Science Foundation, China (No. 2021JJ30854).

References

[1] RITCHIE A G. Recent developments and likely advances in lithium rechargeable batteries [J]. Journal of Power Sources, 2004, 136(2): 285−289.

[2] GRANGE P, DELMON B. The role of cobalt and molybdenum sulphides in hydrodesulphurisation catalysts: A review [J]. Journal of the Less Common Metals, 1974, 36(1/2): 353−360.

[3] LLUSAR M, FORÉS A, BADENES J, CALBO J, TENA M, MONRÓS G. Colour analysis of some cobalt-based blue pigments [J]. Journal of the European Ceramic Society, 2001, 21(8): 1121−1130.

[4] STRNAT K J, STRNAT R M W. Rare earth-cobalt permanent magnets [J]. Journal of Magnetism and Magnetic Materials, 1991, 100: 38−56.

[5] SATO J, OMORI T, OIKAWA K, OHNUMA I, KAINUMA R, ISHIDA K. Cobalt-base high-temperature alloys [J]. Science, 2006, 312(5770): 90−91.

[6] ANTONY K C. Wear-resistant cobalt-base alloys [J]. JOM, 1983, 35(2): 52−60.

[7] DEHAINE Q, TIJSSELING L T, GLASS H J, TÖRMÄNEN T, BUTCHER A R. Geometallurgy of cobalt ores: A review [J]. Minerals Engineering, 2021, 160: 106656.

[8] LEBEDEVA N. Li-ion batteries for mobility and stationary storage applications [M].Luxembourg: Publications Office of the European Union, 2018.

[9] MAKUZA B, TIAN Q H, GUO X Y, CHATTOPADHYAY K, YU D W. Pyrometallurgical options for recycling spent lithium-ion batteries: A comprehensive review [J]. Journal of Power Sources, 2021, 491: 229622.

[10] RUDNICK R L, GAO S. Treatise on geochemistry [M]. Amsterdam: Elsevier, 2014: 1−51.

[11] HUANG Y, ZHANG Z, CAO Y, HAN G, PENG W, ZHU X, ZHANG T A, DOU Z. Overview of cobalt resources and comprehensive analysis of cobalt recovery from zinc plant purification residue—A review [J]. Hydrometallurgy, 2020, 193: 105327.

[12] LIU W F, RAO S, WANG W Y, YANG T Z, YANG L, CHEN L, ZHANG D C. Selective leaching of cobalt and iron from cobalt white alloy in sulfuric acid solution with catalyst [J]. International Journal of Mineral Processing, 2015, 141: 8−14.

[13] CHONG S, HAWKER W, VAUGHAN J. Selective reductive leaching of oxidised cobalt containing residue [J]. Minerals Engineering, 2013, 54: 82−87.

[14] AÇMA E C. The effect of sulfur and reduction temperature on cobalt dissolution during sulfuric acid leaching of metallic matte [J]. Canadian Metallurgical Quarterly, 1997, 36(1): 25−29.

[15] LIU Z J, LIU X, LI L Y, XU S M, WANG X J. Atmospheric leaching of Co white alloy [J]. Nonferrous Metals Science and Engineering, 2015, 6(1): 24−28, 65. (in Chinese)

[16] XIA W T, CHEN X Y, SHI H Y. Extracting Cu, Co, and Fe from white alloy with HCl by adding H_2O_2 [J]. JOM, 2010, 62(11): 49−52.

[17] BURZYŃSKA L, GUMOWSKA W, RUDNIK E. Influence of the composition of Cu−Co−Fe alloys on their dissolution in ammoniacal solutions [J]. Hydrometallurgy, 2004, 71(3/4): 447−455.

[18] FENG R S, XU S M, LIU J, WANG C Y. The influence of Cl^- on the electrochemical dissolution of cobalt white alloy containing high silicon in a sulfuric acid solution [J]. Hydrometallurgy, 2014, 142: 12−22.

[19] JEONG E H, NAM C W, PARK K H, PARK J H. Sulfurization of Fe−Ni−Cu−Co alloy to matte phase by carbothermic reduction of calcium sulfate [J]. Metallurgical and Materials Transactions B, 2016, 47(2): 1103−1112.

[20] REN G X, LIU Z H, PAN B, XIAO S W. A novel process for cobalt and copper recovery from cobalt white alloy with high silicon [J]. Metallurgical Research & Technology, 2020, 117: 404. (in Chinese)

[21] GUO X Y, ZHANG C X, TIAN Q H, YU D W. Liquid metals dealloying as a general approach for the selective extraction of metals and the fabrication of nanoporous metals: A review [J]. Materials Today Communications, 2021, 26: 102007.

[22] OKABE T H, TAKEDA O, FUKUDA K, UMETSU Y. Direct extraction and recovery of neodymium metal from

magnet scrap [J]. Materials Transactions, 2003, 44(4): 798−801.
[23] YAGI R, OKABE T H. Recovery of nickel from nickel-based superalloy scraps by utilizing molten zinc [J]. Metallurgical and Materials Transactions B, 2016, 48(1): 335−345.
[24] ZHANG C X, GUO X Y, YU D W, TIAN Q H, CUI F H. Treatment of copper-cobalt alloy with molten magnesium for metal extraction [J]. Journal of Alloys and Compounds, 2021, 874: 159933.
[25] OKAMOTO H, MASSALSKI T B. Binary alloy phase diagrams [M]. Materials Park, OH, USA: ASM International, 1990.
[26] BALE C W, BÉLISLE E, CHARTRAND P, DECTEROV S A, ERIKSSON G, GHERIBI A E, HACK K, JUNG I H, KANG Y B, MELANÇON J, PELTON A D, PETERSEN S, ROBELIN C, SANGSTER J, SPENCER P, van ENDE M A. FactSage thermochemical software and databases, 2010−2016 [J]. Calphad, 2016, 54: 35−53.
[27] IIDA T, KITA Y, OKANO H, KATAYAMA I, TANAKA T. An equation for the vapor pressure of liquid metals and calculation of their enthalpies of evaporation [J]. High Temperature Materials and Processes, 1992, 10(4): 199−208.
[28] OLESINSKI R W, ABBASCHIAN G J. The Pb−Si (lead−silicon) system [J]. Bulletin of Alloy Phase Diagrams, 1984, 5(3): 271−273.
[29] RISOLD D, NAGATA J I, SUZUKI R O. Thermodynamic description of the Pb−O system [J]. Journal of Phase Equilibria, 1998, 19(3): 213−233.
[30] NAYEB-HASHEMI A A, CLARK J B. The Cu−Mg (copper−magnesium) system [J]. Bulletin of Alloy Phase Diagrams, 1984, 5(1): 36−43.
[31] RAMBALDI G, MAZZONE D, MARAZZA R, DELFINO S, FERRO R. Phase equilibria in the Mg-rich corner of the magnesium−copper-lead system [J]. Journal of the Less Common Metals, 1978, 59(2): 201−210.
[32] SCHNEIDER C A, RASBAND W S, ELICEIRI K W. NIH Image to ImageJ: 25 years of image analysis [J]. Nature Methods, 2012, 9(7): 671−675.
[33] TANAKA Y, KAJIHARA M, WATANABE Y. Growth behavior of compound layers during reactive diffusion between solid Cu and liquid Al [J]. Materials Science and Engineering A, 2007, 445/446: 355−363.
[34] SAKAMA T, KAJIHARA M. Kinetics of reactive diffusion between Pd−Ag alloys and Sn at solid-state temperatures [J]. Journal of Alloys and Compounds, 2009, 475(1/2): 608−613.
[35] OSAMURA K, OCHIAI S, KONDO S, NAMATAME M, NOSAKI M. Influence of third elements on growth of Nb_3Sn compounds and on global pinning force [J]. Journal of Materials Science, 1986, 21(5): 1509−1516.

利用镁铅熔体的协同选择性从铜钴合金中提取铜

张纯熹，于大伟，郭学益，田庆华

中南大学 冶金与环境学院，长沙 410083

摘　要：使用镁铅二元熔体高效、选择性地从铜钴合金中提取铜。确定提取铜的最佳反应条件。结果表明，在反应温度为 800 ℃、反应时间为 1 h 的最佳条件下，铜的提取率高达 96.5%，而铁、钴和硅的提取率分别仅为 0.2%、0.6%和 1.4%。铜的溶解机理主要是镁/铅与铜在铜钴合金溶解区域的对向扩散，且镁铅二元熔体中镁在铜的选择性溶解中起主要作用(特别是在溶解前沿位置)。界面反应为提取过程的速度控制步骤。

关键词：Cu−Co 合金；Mg−Pb−Cu 三元体系；选择性溶解；动力学；去合金化

(Edited by Wei-ping CHEN)